Cryoelectron Microscopy of a Nucleating Model Bile in Vitreous Ice: Formation of Primordial Vesicles

Donald L. Gantz,* David Q.-H. Wang,# Martin C. Carey,# and Donald M. Small*

*Department of Biophysics, Boston University School of Medicine, Boston, Massachusetts 02118, and #Department of Medicine, Gastroenterology Division, Brigham and Women's Hospital, Harvard Medical School and Harvard Digestive Disease Center, Boston, Massachusetts 02115 USA

ABSTRACT Because gallstones form so frequently in human bile, pathophysiologically relevant supersaturated model biles are commonly employed to study cholesterol crystal formation. We used cryo-transmission electron microscopy, complemented by polarizing light microscopy, to investigate early stages of cholesterol nucleation in model bile. In the system studied, the proposed microscopic sequence involves the evolution of small unilamellar to multilamellar vesicles to lamellar liquid crystals and finally to cholesterol crystals. Small aliquots of a concentrated (total lipid concentration = 29.2 g/dl) model bile containing 8.5% cholesterol, 22.9% egg yolk lecithin, and 68.6% taurocholate (all mole %) were vitrified at 2 min to 20 days after fourfold dilution to induce supersaturation. Mixed micelles together with a category of vesicles denoted primordial, small unilamellar vesicles of two distinct morphologies (sphere/ellipsoid and cylinder/arachoid), large unilamellar vesicles, multilamellar vesicles, and cholesterol monohydrate crystals were imaged. No evidence of aggregation/fusion of small unilamellar vesicles to form multilamellar vesicles was detected. Low numbers of multilamellar vesicles were present, some of which were sufficiently large to be identified as liquid crystals by polarizing light microscopy. Dimensions, surface areas, and volumes of spherical/ellipsoidal and cylindrical/arachoidal vesicles were quantified. Early stages in the separation of vesicles from micelles, referred to as primordial vesicles, were imaged 23–31 min after dilution. Observed structures such as enlarged micelles in primordial vesicle interiors, segments of bilayer, and faceted edges at primordial vesicle peripheries are probably early stages of small unilamellar vesicle assembly. A decrease in the mean surface area of spherical/ellipsoidal vesicles was correlated with the increased production of cholesterol crystals at 10–20 days after supersaturation by dilution, supporting the role of small unilamellar vesicles as key players in cholesterol nucleation and as cholesterol donors to crystals. This is the first visualization of an intermediate structure that has been temporally linked to the development of small unilamellar vesicles in the separation of vesicles from micelles in a model bile and suggests a time-resolved system for further investigation.

INTRODUCTION

The structures and mechanisms involved in cholesterol solubility and cholesterol crystal formation in human bile have been investigated for many years in the attempt to understand human gallstone formation (Cabral and Small, 1989; Carey and Small, 1978; Small, 1980; Wang and Carey, 1996a). Structural information about cholesterol carriers in pathophysiologically relevant model bile systems (Cohen et al., 1993; Gilat and Sömjen, 1996) as well as crystallization has been provided by a number of techniques such as quasielastic light scattering (Cohen et al., 1990; Little et al., 1991; Mazer et al., 1980; Mazer and Carey, 1983), small-angle x-ray scattering (Sömjen, 1994), small-angle neutron scattering (Hjelm et al., 1992; Long et al., 1994a), video-enhanced contrast microscopy (Halpern et al., 1986a), polarizing light microscopy (Konikoff and Carey, 1994; Konikoff et al., 1992; Wang and Carey, 1996a,b), and electron microscopy techniques such as negative staining (Groen et al., 1989; Sömjen et al., 1990b; Tao et al., 1993), freeze fracturing (Sömjen et al., 1986; van de Heijning et al., 1994), and vitreous ice cryomicroscopy (Kaplun et al., 1997, 1994; Vinson et al., 1989; Walter et al., 1991). The electron microscopy technique in vitreous ice (Dubochet et al., 1988) can provide images of particles and structures in lipid-rich systems that are believed to be close to their original state in solution. Utilizing this technique, we have attempted to detect the earliest stages of nucleation, visualizing all structures present in a supersaturated, nucleating model bile from initial formation to 20 days after supersaturation, and to correlate ultrastructural observations with those made with polarizing light microscopy. In the earliest stage, we have obtained images of the nucleation of micelles into primordial vesicles.

MATERIALS AND METHODS

Chemicals

Grade A taurocholate (Sigma Chemical Co., St. Louis, MO) was purified by the method of Pope (1967) and found to be >99% pure by high-performance liquid chromatography (HPLC). Cholesterol (Nu-Chek Prep., Elysian, MN) and grade I egg yolk lecithin (Lipid Products, South Nutfield, Surrey, England) were found to be >99% pure by gas-liquid chromatography, thin-layer chromatography, and HPLC. All other chemicals and solvents were American Chemical Society (ACS) or reagent grade quality (Fisher Scientific Co., Medford, MA).

Received for publication 9 March 1998 and in final form 4 November 1998.

Address reprint requests to Mr. Donald L. Gantz, Department of Biophysics, W301, Boston University School of Medicine, 715 Albany Street, Boston, MA 02118. Tel: 617-638-4017; Fax: 617-638-4041; E-mail: gantz@med-biophd.bu.edu.

0006-3495/99/03/1436/16 $2.00

Preparation of model bile

Model micellar bile was prepared by coprecipitation of cholesterol, lecithin, and taurocholate from $CHCl_3$-MeOH (2:1, v/v) to yield a relative composition of 8.5%, 22.9%, and 68.6%, respectively (all mole %). The total lipid concentration was 29.2 g/dl. Lipid mixtures were dried under a stream of N_2 and then under reduced pressure for 24 h to achieve constant weight. Each dried lipid film was then dissolved in aqueous solution (0.15 M NaCl adjusted with 1–2 μl of 1 M NaOH to pH 7.0), containing 3 mM NaN_3 as an antimicrobial agent. After the tubes were sealed under a blanket of N_2 with Teflon-lined screw caps, they were vigorously vortex-mixed for a few minutes. To ensure complete solubilization of coprecipitated cholesterol in micelles, the model bile was shaken at 100 rpm for 1 h at 50°C, using a model 75 Wrist Action Shaker (Burrell Corporation, Pittsburgh, PA). The stock bile solution was then microfiltered at 22°C through a preheated Swinnex-GS filter assembly containing a 0.22-μm filter (Millipore Products Division, Bedford, MA), and ~0.1 ml of sample was aspirated for later lipid analysis (see below). To induce supersaturation, stock solutions were diluted fourfold with 0.15 M NaCl (pH 7.0) to 7.3 g/dl. According to critical tables (Carey, 1978), with the assumption that the intended cholesterol composition was correct (see Wang and Carey, 1996b), this dilution should increase the cholesterol saturation index (CSI) from 0.97 ± 0.03 to 1.21 ± 0.05 (see Lipid Analysis below). The dilution time point was taken as the initiation of all nucleation studies (Wang and Carey, 1996a). Fig. 1 indicates that this model bile at equilibrium falls in a central three-phase zone, region C, containing saturated micelles, liquid crystals, and cholesterol monohydrate crystals, with a microscopic crystallization sequence of micelles → liquid crystals → cholesterol monohydrate crystals → anhydrous cholesterol crystals, which is well defined (Wang and Carey, 1996a).

Monitoring of crystallization sequences by polarizing light microscopy

The nucleating biles were sealed in glass test tubes, blanketed with N_2, and incubated at room temperature (22 ± 1°C). Crystallization sequences were verified by the method of Wang and Carey (1996a). No differences in crystallization sequences were observed if the sample was shaken before sampling or left undisturbed. In brief, 5-μl samples were taken from the bottom third of a 4-ml model bile sample and placed immediately on a glass slide at room temperature (22 ± 1°C). Samples were observed initially without a coverslip by polarized light microscopy (Photomicroscope III; Carl Zeiss, Thornwood, NY) at 400× magnification. The sample was then compressed with a cover glass and reexamined with phase-contrast optics. New slides were examined at 2-h intervals for 12 h, and then daily for 20 days to determine crystallization sequences. Detection times of cholesterol crystals and liquid crystals were defined as the time from initial dilution to the earliest microscopic detection at 400× of arc, helical, tubular, cholesterol monohydrate, or small, aggregated, and fused liquid crystals (Wang and Carey, 1996a).

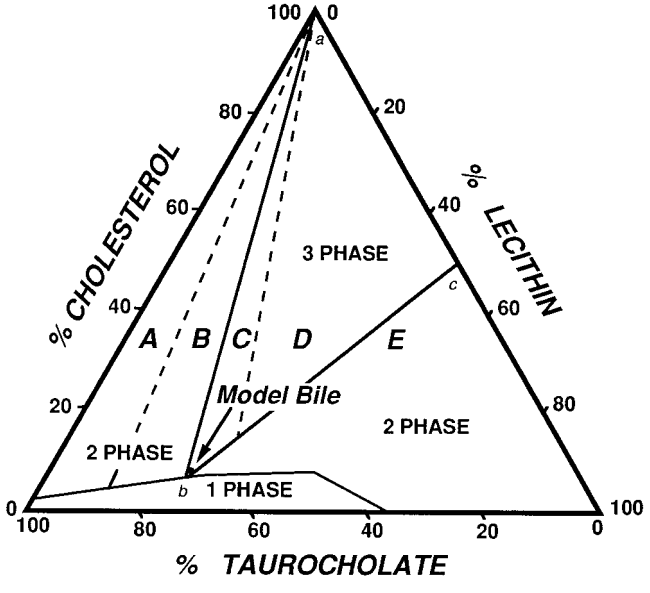

FIGURE 1 Equilibrium phase diagram of taurocholate-lecithin-cholesterol system (total lipid concentration = 7.3 g/dl, 0.15 M NaCl, pH 7.0, 22°C) used in this study. Composition was 68.6% taurocholate, 22.9% lecithin, and 8.5% cholesterol (mole %), placing it in region C of the central three-phase zone (●). The three phases at equilibrium are saturated micelles, liquid crystals, and cholesterol monohydrate crystals (see Fig. 2 for crystallization sequences).

Lipid analysis

Taurocholate concentrations were assayed by the 3α-hydroxysteroid dehydrogenase method (Turley and Dietschy, 1978); lecithin by an inorganic phosphorus procedure (Bartlett, 1959); and cholesterol enzymatically (Fromm et al., 1980). Calculation of CSIs for model bile was based on the critical tables (Carey, 1978).

Cryo-transmission electron microscopy

Model bile was incubated at 22°C in a 15 × 100 mm screw cap glass culture tube (Kimble/Kontes, Vineland, NJ) on a bench top during each experiment (20 days). The model bile initially extended to a height of 3 cm in the tube. The tube was hand-shaken for ~30 s just before sampling or was left undisturbed. Each 7-μl aliquot was removed with a Gilson P20 pipetteman (Villiers-le-Bel, France) at a height of 0.8 cm from the tube's base and placed on a freshly glow-discharged (Dubochet et al., 1982) holey carbon film covering a 400 mesh copper grid (Electron Microscopy Sciences, Fort Washington, PA), which was gripped by forceps held closed by a rubber ring. The forceps were then attached to a nitrogen gas-driven plunger (Charles Ingersoll Corp., Winthrop, MA) inside a plexiglas freezing station (Dan-Kar Corp., Reading, MA) of dimensions 21″ × 21″ × 31″ (height) with a vertically sliding access door of dimensions 15″ × 9″ (height). This door was kept closed except when a sample was loaded, a grid was blotted, or a grid was transferred to a storage box. Humid air produced by an Ultrasonic Humidifier (model TUH-420; Tatung Company of America, Long Beach, CA) entered at the rear of the freezing station through a 1.5″-diameter flexible hose. The atmosphere in the chamber became foggy, particularly over the container of liquid nitrogen where the forceps were hung. Humidity was monitored with a Vaisala Humidity Meter (Vaisala Co., Helsinki, Finland). The humidity dipped slightly below 100% when the access door was opened during blotting. Samples were blotted from the underside (not the sample side) with oven-dried no. 1 filter paper (Whatman Paper Limited, Kent, England) and plunged, by activating a pedal, into a liquid ethane-filled stainless steel cup partially submerged in liquid nitrogen. Because the temperature of liquid nitrogen (77 K) is below the freezing point of ethane (90 K), the ethane slowly solidified from the inside surface of the cup toward the center. Each grid was plunged after a thin layer of solid ethane had appeared, ensuring that the remainder of the liquid ethane was close to its freezing point. Underside blotting (Toyoshima, 1989) was used to concentrate particles. Pilot experiments indicated that 1–10 s between blotting and plunging in the humidified environment would provide suitable vitreous ice thicknesses. During the first 30 min after supersaturation, grids were prepared as quickly as possible, resulting in the time points shown in Table 1. At time points of 6 h and 1, 4, 10, and 20 days, several grids were prepared with postblotting/preplunging times of 1, 5, and 10 s. Estimates of cooling times required to produce vitreous ice from thin liquid films such as ours range from 2 ms (Klösgen and Helfrich, 1993) to an optimum of 0.1 ms (Dubochet et al., 1988). Vitrified samples were stored in a cryogenic storage dewar (Taylor-Wharton, Theodore, AL) under liquid nitrogen.

TABLE 1 Particles and crystals observed in nucleating model bile by cryo-TEM at various times after supersaturation*

Time	Micelles	PVs#	SUVs		LUVs	MLVs	ChM crystals
			SEVs	CAVs			
2 min	+	−	−	−	−	−	−
5 min	+	−	−	−	−	−	−
9 min	+	−	−	−	−	−	−
13 min	+	−	−	−	−	−	−
23 min	+	+	−	−	−	−	−
27 min	+	+	−	+§	−	−	−
31 min	+	+	−	−	−	−	−
6 h	+	+	+	+	−	−	−
1 day	+	−	+	+	+	+	−
4 days	+	+	+	+	+	+	−
10 days	+	−	+	+	+	−	+
20 days	+	−	+	+	+	+	+

*Sample tube was shaken prior to sampling; (+), present; (−), absent.
#PVs, primordial vesicles; SUVs, small unilamellar vesicles; SEVs, spherical/ellipsoidal vesicles; CAVs, cylindrical/arachoidal vesicles; LUVs, large unilamellar vesicles; MLVs, multilamellar vesicles; ChM, cholesterol monohydrate.
§Only one CAV was seen in 15 fields.

Vitrified samples were transferred into a Single Tilt Cryoholder (model 626), using a Cryotransfer Station (Gatan, Pleasanton, CA). The cryoholder maintained samples at 99 K while images were recorded at a defocus value of 1.4 μ on SO-163 electron image film (Eastman Kodak Co., Rochester, NY) in a Philips CM-12 transmission electron microscope (Philips Electron Optics, Eindhoven, The Netherlands) equipped with a low-dose kit to minimize irradiational damage. Edges and centers of large holes and entire small holes were photographed. The scope was calibrated with a silicon monoxide grating replica (Ernest F. Fullam, Latham, NY). Micrographs were developed in full-strength D19 (Eastman Kodak Co.) for 12 min. Images of vesicles at 0° and 45° tilt were compared to confirm three-dimensional morphology.

Particle measurements were made with a Peak 7× magnifier with a 1–20-mm graticule in 0.1-mm divisions on micrographs enlarged 2.5× on resin-coated paper. At each time point, particles were analyzed from at least 18 vitreous ice-containing holes to a maximum of 81 holes. Ice at hole edges was thicker than ice in hole centers, but among all holes inspected no data were obscured.

For negative staining a 30-μl aliquot of model bile sampled in the same manner as vitreous ice was mixed with 10 μl of 2% osmium tetroxide in 0.1 M phosphate buffer (pH 7.3), giving a final OsO_4 concentration of 0.5%. After a 20-min fixation to stabilize lipid structures, a 10-μl aliquot was placed on a glow-discharged (Dubochet et al., 1982) carbon, formvar-coated 300 mesh copper grid, stained with 1% sodium phosphotungstate (1% NaPT, pH 7.3), blotted, and air-dried.

Classification of vesicle morphology

Vesicle-like particles that had curved or straight single strands and/or an occasional bilayer fragment that formed a discontinuous circular to oval outline sufficient for diameter measurement were considered a new category of vesicle. These were called "primordial vesicles." Small unilamellar vesicles were completely formed and had distinct, well-defined continuous bilayers. Each small unilamellar vesicle was assigned to one of two morphological categories based on its two-dimensional projection: spherical/ellipsoidal vesicle or cylindrical/arachoidal vesicle. The morphologies of small unilamellar vesicles were confirmed by 45° tilt images. A vesicle with a circular or oval-shaped projection was a sphere or ellipsoid, respectively. A vesicle with a projection of constant width along its entire length was a cylinder. A vesicle having a peanut-shaped projection with at least one end of greater width than its center was an arachoid. A number of parameters determining vesicle shape have been discussed in detail by Mui et al. (1995).

Calculation of surface area and volume of small unilamellar vesicles

The following formulae (Frame, 1992) were used to calculate the surface area and volume of small unilamellar vesicles:

Surface area of spherical vesicle = $4\pi r^2$

Surface area of ellipsoidal vesicle = $2\pi(r_1)^2 + 2\pi(r_2 r_1 \div e)\arcsin(e)$, where r_1 is the minor radius, r_2 is the major radius, and e (eccentricity) = the square root of $[1 - (r_1)^2 \div (r_2)^2]$.

Surface area of cylindrical vesicle = $\pi dL + 2\pi r^2$, where d is the diameter of the vesicle and L is the length of the vesicle.

Surface area of arachoidal vesicle = $\pi d(\text{avg})L + 2\pi r^2(\text{avg})$, where $d(\text{avg}) = [d(\text{min}) + 2d(\text{max})] \div 3$, $d(\text{min})$ is the smallest width at the center of the vesicle, $d(\text{max})$ is the mean of the largest width at each end of the vesicle, and $r(\text{avg}) = d(\text{avg}) \div 2$.

Volume of spherical/ellipsoidal vesicles = $(4/3)\pi(r_1^2)$.

Volume of cylindrical/arachoidal vesicles = $\pi r^2(\text{avg})L$.

Statistical methods

All data are expressed as means ± SD. Statistical methods, including parametric and nonparametric tests, χ^2, and least-squares regression analyses were performed with an RS1 software package, release 4.3.1, 1991 (BBN Software Products Corporation, Cambridge, MA). Statistical significance was defined as a two-tailed probability less than 0.05.

RESULTS

Crystallization sequences by polarizing light microscopy

The time sequences of the appearance and disappearance of liquid crystals, cholesterol monohydrate crystals, arcs, helices, and tubular crystals in this model bile system as observed by light microscopy are shown in Fig. 2 *A*. Each type of crystal is illustrated in Fig. 2 *B*. Small, aggregated, and fused liquid crystals (Fig. 2 *B*: *1*, *2*, *3*) were detected first at 1, 2, and 3 days, respectively, after fourfold dilution to induce supersaturation. They peaked at 6, 7, and 9 days and disappeared at 14, 15, and 16 days, respectively. Cholesterol monohydrate crystals (Fig. 2 *B*: *4*) were first observed at 4 days and peaked at 17 days. Arc, helical, and tubular crystals (Fig. 2 *B*: *5*, *6*, *7*, *8*) were initially detected at 11, 12, and 13 days and peaked at 16, 17, and 18 days, respectively. Detailed information on crystallization pathways in model biles of similar composition has been published (Wang and Carey, 1996a). No appreciable differences were observed in the crystallization sequences when samples were taken from an unshaken tube of model bile or from a tube shaken just before bile was sampled.

Particles observed by cryo-transmission electron microscopy

Six types of nucleating particles and cholesterol monohydrate crystals were visualized by vitreous ice electron mi-

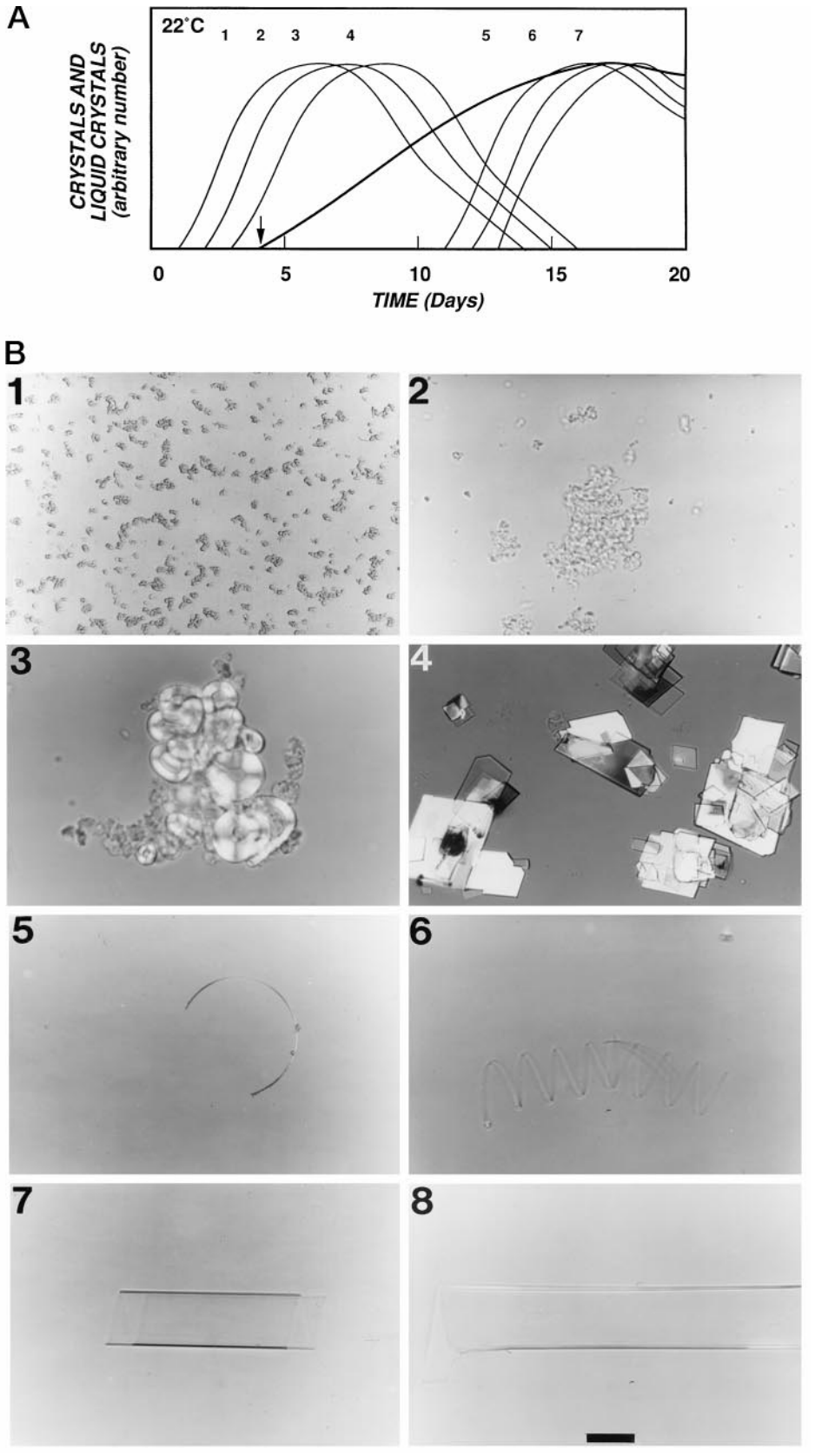

FIGURE 2 Based on the principal characteristics of the phases for the above model bile, its crystallization sequence was in crystallization pathway C (Wang and Carey, 1996a). (*A*) The vertical axis represents arbitrary numbers of crystals and liquid crystals per microscopic field at ×400 magnification, all normalized to the same maximum. Consecutive numbers represent small (*1*), aggregated (*2*), and fused (*3*) liquid crystals, plate-like cholesterol monohydrate crystals (*4*), and arc-shaped (*5*), helical (*6*), and tubular (*7*) crystals. The arrow indicates the first detection of cholesterol monohydrate crystals. (*B*) Characteristics of liquid and solid crystals of cholesterol observed by polarizing light microscopy in this study: (*1*) small nonbirefringent liquid crystals; (*2*) nonbirefringent aggregated liquid crystals; (*3*) typical fused liquid crystals with Maltese cross birefringence and focal conic textures; (*4*) typical cholesterol monohydrate crystals, with 79.2° and 100.8° angles, and frequent notched corners; (*5*) arc-like (possibly anyhydrous cholesterol) crystal; (*6*) regular right-handed helical crystals; (*7*) tubular crystal; and (*8*) tubular crystal fracturing at the ends to produce plate-like cholesterol monohydrate crystal. All magnifications are ×800. Bar = 10 μm.

croscopy: 1) micelles—mostly ovoid/barrel-shaped particles of mean width and length (nm ± SD) of 3.6 ± 1.1 and 5.6 ± 1.6, respectively (n = 98); 2) primordial vesicles—an early stage in the formation of spherical/ellipsoidal vesicles in which a discontinuous circular or oval outline apparently formed by short segments of bilayer fragments is visible; 3)

small unilamellar vesicles—two morphologically unique categories of small unilamellar vesicles, spherical/ellipsoidal vesicles, and cylindrical/arachoidal vesicles, with distinct bilayers and mean diameters less than 100 nm; 4) large unilamellar vesicles—vesicles with distinct bilayers and mean diameters greater than 100 nm; 5) multilamellar vesicles—vesicles with more than one bilayer; and 6) cholesterol monohydrate crystals—large platelike crystals with unique edge angles of 79.2° and 100.8°. Attempts at obtaining images of undiluted model bile at ~30 g/dl were unsuccessful because vitreous ice layers were too dense. No particles were seen in buffer (0.15 M NaCl, pH 7.0) alone (micrograph not shown).

The dispersed particles and crystals observed at various time points after supersaturation are enumerated in Table 1. In this experiment, the sample tube was shaken for 30 s just before removal of an aliquot for vitrification.

Micelles were present at all time points and are illustrated in Fig. 3 *A*. Ranges of width and length were 1.1–5.7 nm and 2.3–10.3 nm, respectively ($n = 98$). Circular regions of reduced micelle granularity (Fig. 3 *A*, *between arrows*) may represent the beginning stage of vesicle formation. At higher magnification (Fig. 3 *A*, *inset*) the morphology of the nucleating micelles appeared rectangular with some squares (rare rounded ends), suggesting barrel-shaped particles and not discs.

Primordial vesicles were first detected 23 min after supersaturation (Table 1, Fig. 3 *B*). Primordial vesicles were generally round to slightly oval in shape. Their interiors appeared slightly more dense but less granular than surrounding ice with only micelles (a projection through two partially formed membranes would likely increase density) and contained angular structures (with rare exceptions) of mean width and length (nm ± SD) of 4.4 ± 1.8 and 6.2 ± 1.9, respectively ($n = 34$), a size similar to micelles (Fig. 3 *B*). The width and length ranges of these angular structures were 1.1–8.0 nm and 3.4–10.3 nm, respectively. At 27 min (Fig. 3 *C*), several of the primordial vesicles had boundaries partially defined by short segments of bilayer (ranging from 2.3 to 4.6 nm in thickness) and by curved or straight single strands. These strands are probably not monolayers because monolayers would be very unstable and are not likely to be imaged. The end-to-end contact of several straight segments at obtuse angles gave a faceted appearance to some of the boundaries (Fig. 3 *C*). Primordial vesicles were also observed at 6 h and 4 days (rare), but not at 1, 10, and 20 days after supersaturation by dilution (Table 1). The mean width and length (nm ± SD) of primordial vesicles at 23 min was

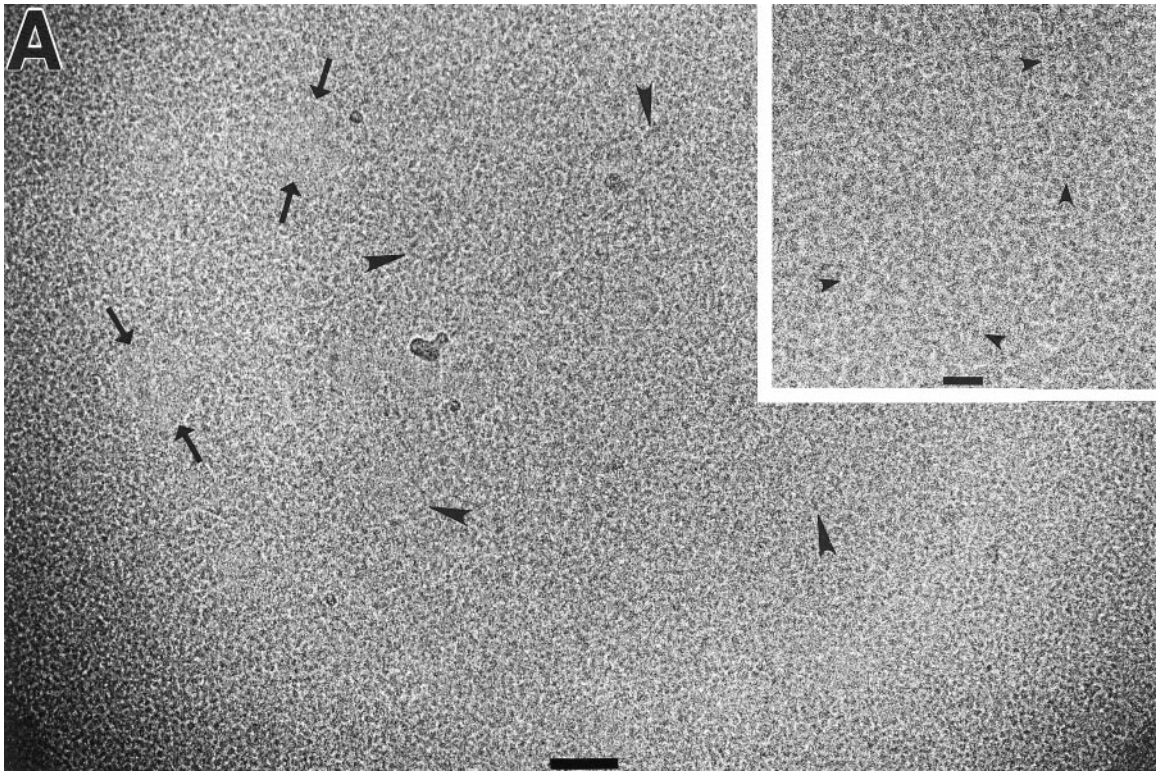

FIGURE 3 Here and next two pages. Cryo-transmission electron microscopy micrographs of mixed micelles, primordial vesicles, spherical/ellipsoidal vesicles, and cylindrical/arachoidal vesicles observed in model bile vitrified at various time points after supersaturation by dilution (see Table 1). Micelles were present at all time points. See Tables 2 and 3 for mean sizes of primordial vesicles and small unilamellar vesicles, respectively. Regions of higher density near hole edges indicate thicker ice. In *A–E*, bars = 50 nm. (*A*) At 2 min, mixed micelles of width and length (mean ± SD) of 3.6 ± 1.1 and 5.6 ± 1.6 nm were clearly seen at the hole periphery. Thin, curved threadlike structures (*arrowheads*) were visible toward the hole center. Circular areas of reduced micelle granularity (*between arrows*) may be a very early stage in the vesicle development. (*Inset*) Micelles at higher magnification in a hole interior at 2 min appeared square to rectangular (*arrowheads*), suggesting a barrel-shaped morphology. Bar = 25 nm.

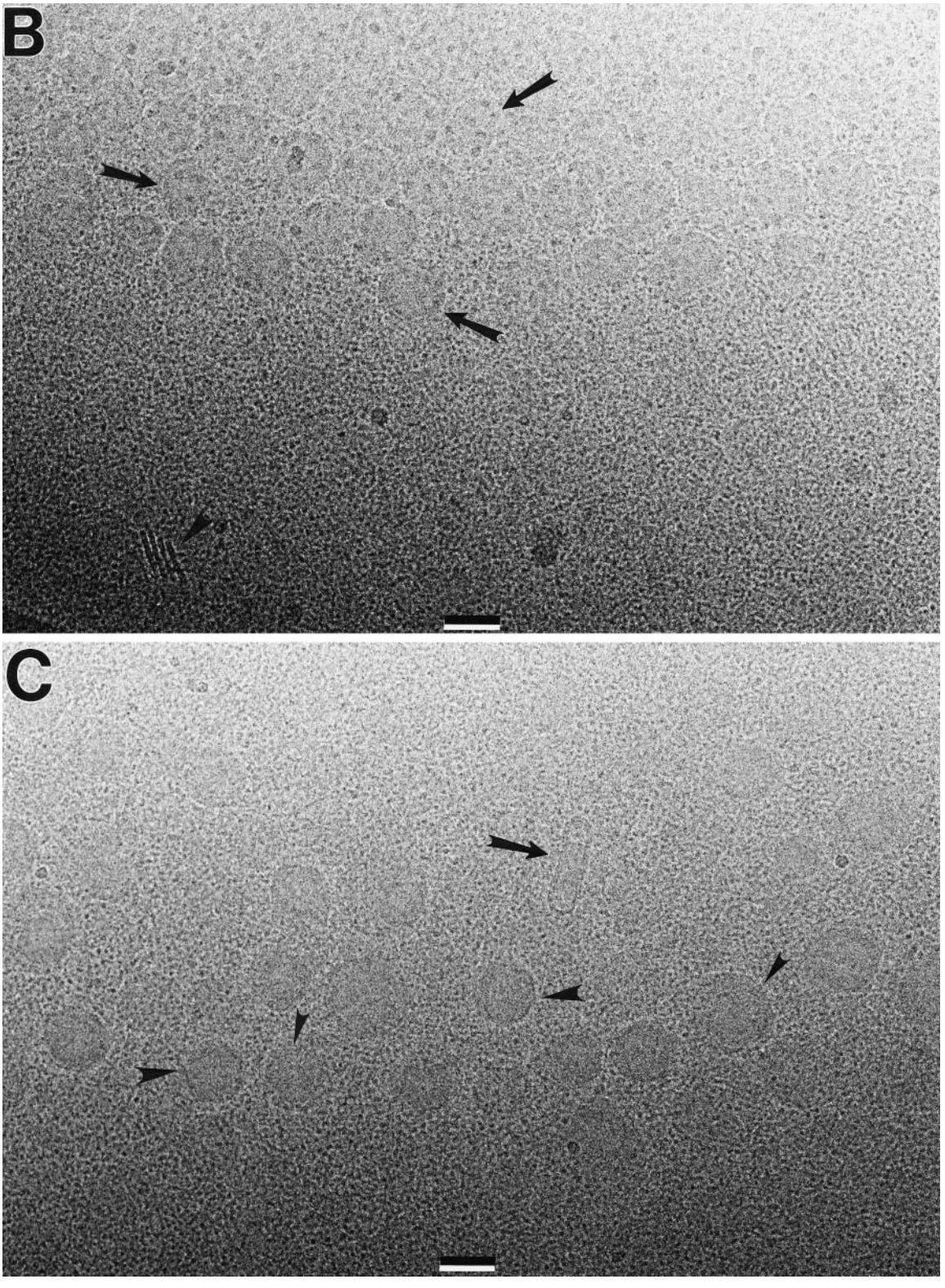

FIGURE 3 (*Continued*). (*B*) At 23 min, primordial vesicles (*arrows*) were present and contained angular structures that were slightly larger than micelles (see interiors). Also visible was an extremely rare cluster of lamellae (*arrowhead*). (*C*) At 27 min, primordial vesicles had slightly more well-defined boundaries, some of which appeared faceted (*large arrowheads*). Occasional short bilayer segments at vesicle peripheries were visible (*small arrowheads*). One cylindrical/arachoidal vesicle (*arrow*) was detected at this time point. No primordial cylindrical/arachoidal vesicles were ever seen.

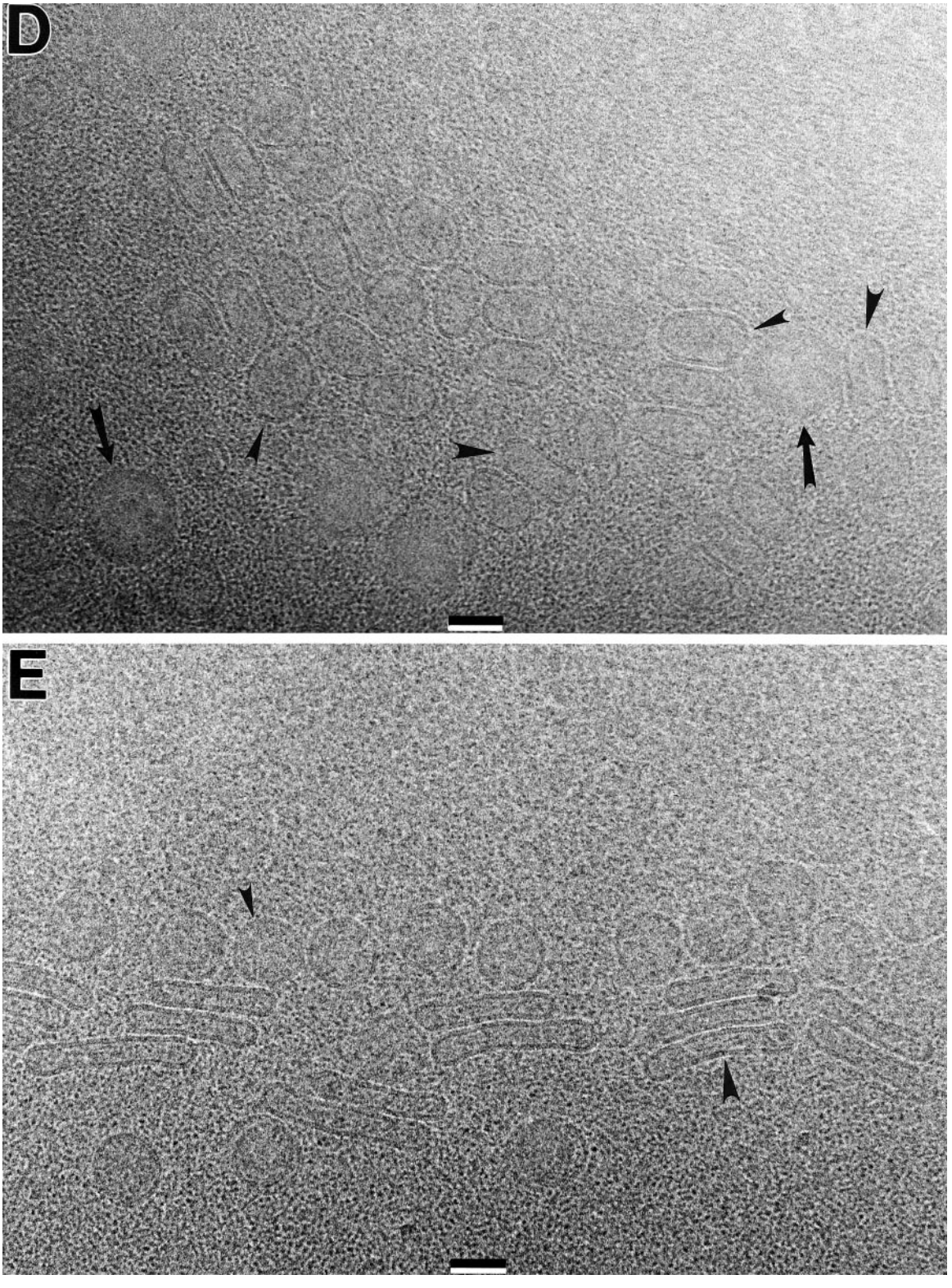

FIGURE 3 (*Continued*). (D) At 6 h, spherical/ellipsoidal vesicles (*small arrowheads*) and cylindrical/arachoidal vesicles (*large arrowheads*) with well-defined bilayers were prevalent. Primordial vesicles (*arrows*) and micelles were interspersed. (*E*) Small unilamellar vesicles were frequently observed in ranks arranged concentrically within a hole (spherical/ellipsoidal vesicles, *small arrowhead*; cylindrical/arachoidal vesicle, *large arrowhead*). Thinner ice is located toward the top.

47 ± 7.4 and 52 ± 8.6, respectively (Table 2). There was no significant increase in the mean size of primordial vesicles at 27 and 31 min, but primordial vesicles at 6 h and 4 days were significantly larger. Although a few round primordial vesicles were seen at each of the above time points, the mean shape was oval, because the mean width was significantly different from the mean length at all time points (Table 2).

Although two groups of bilayer-like structures were observed in our study, they were extremely rare (only two in over 450 photographed holes). A group of four such structures detected at 23 min (Fig. 3 *B*) had a range of thicknesses of 4.6–5.7 nm and lengths of 40–45 nm. The other group, observed at 10 days (not shown), contained structures with a thickness of 6 nm and a range of lengths of 57–97 nm.

Although the exact time point when small unilamellar vesicles first appeared was not determined, at 6 h small unilamellar vesicles with distinct bilayers were common (Fig. 3 *D*). These vesicles could be divided into two morphologically distinct categories: spherical/ellipsoidal vesicles and cylindrical/arachoidal vesicles (see Materials and Methods for details). Three-dimensional morphologies were confirmed by 45° tilt images (not shown). Bilayer thicknesses of spherical/ellipsoidal vesicles and cylindrical/arachoidal vesicles ranged from 3.4 to 5.7 nm. Both vesicle morphologies were commonly found at each of four subsequent time points (Table 1). Some primordial vesicles were interspersed among spherical/ellipsoidal vesicles and cylindrical/arachoidal vesicles (Fig. 3 *D*). Spherical/ellipsoidal vesicles and cylindrical/arachoidal vesicles were frequently in rows or ranks positioned in concentric rings from thinner to thicker ice within a hole (Fig. 3 *E*). One arachoid vesicle was observed at 27 min (Fig. 3 *C*), the only arachoid detected during the first 31 min after supersaturation by dilution among 120 photographed holes.

Large unilamellar vesicles and multilamellar vesicles were first detected at 1 day after supersaturation (Table 1) and increased slightly in number up to the final time point of 20 days (data not shown). These vesicles were most commonly seen at hole edges where ice was thicker (Fig. 4, *A–C*). Multilamellar vesicles of spherical/ellipsoidal and cylindrical/arachoidal morphologies were present at each time point but not in sufficient numbers to analyze relative frequencies. Diameters of observed large unilamellar vesicles ranged from 140 to 500 nm; those of multilamellar vesicles ranged from 55 nm to over 1 μm. The mean bilayer thickness of large unilamellar vesicles was 5.8 nm (Fig. 4 *B*); that of multilamellar vesicles was 6.4 nm (Fig. 4 *C*). Multilamellar vesicles were occasionally seen inside large unilamellar vesicles (Fig. 4 *B*). Multilamellar vesicles observed by cryo-transmission electron microscopy at 1 day such as that shown in Fig. 4 *A* were not large enough to be visible by polarizing light microscopy (light microscopy could detect crystals as small as 500 nm). Larger multilamellar vesicles such as one with dimensions of 640 nm × 850 nm (Fig. 4 *C*) are potentially detectable by polarizing light microscopy (Wang and Carey, 1996a; see Fig. 2).

Large crystals were observed at 10 and 20 days after dilution (Fig. 4 *D*). The edge angles of these thin platelike crystals were 79.2° and 100.8°, like those reported for cholesterol monohydrate (Small, 1986). The dimensions of the plate in Fig. 4 *D* are 8 μm × 21 μm. Frequently, these plates appeared to be stacked upon one another. A thin, partially coiled structure appeared to be either superimposed upon the image of the plate or associated with the plate. This coiled structure might be similar to arclike or helical structures seen by others using light microscopy and cryo-transmission electron microscopy (Kaplun et al., 1994; Konikoff et al., 1992; Wang and Carey, 1996a), or could be the growth face of the crystal with a growth spiral starting in a screw dislocation (Toor et al., 1978).

Another experiment using a model bile with the same composition but with samples taken from an undisturbed tube yielded qualitatively similar results in vitreous ice (data not shown), with the exception that large unilamellar vesicles and cholesterol monohydrate crystals were not observed (compare Table 1). Failure to see large unilamellar vesicles and cholesterol monohydrate crystals may be attributable to heterogeneous distribution in the undisturbed sample tube (cholesterol density of 1.056 g/ml promotes settling; Konikoff and Carey, 1994) and to the low probability of capture in thin vitreous ice layers.

Negatively stained preparations of model bile sampled at 2 and 10 days after supersaturation produced structures completely different from those seen in vitreous ice (Fig. 5). These lamellar-like structures were stacks of straight to slightly curved discs or sheets of bilayer. Bilayer thicknesses ranged from 5.0 to 5.3 nm. Widths of individual discs in stacks ranged from 16 to 117 nm.

TABLE 2 Mean dimensions of primordial vesicles

Time	*n*	Width*	Length*
23 min	32	47.1 ± 7.4	52.7 ± 8.6[#]
27 min	52	48.6 ± 6.3	53.1 ± 6.6[#]
31 min	152	48.8 ± 9.4	54.8 ± 9.5[#]
6 h	56	74.0 ± 8.9[§]	78.7 ± 8.5[#§¶]
4 days	9	80.2 ± 8.3[§]	86.0 ± 6.8[#§]

*Data are expressed as mean nm ± SD.
[#]$p < 0.005$ compared to vesicle width.
[§]$p < 0.01$ compared to 23, 27, and 31 min.
[¶]$p < 0.05$ compared to 4 days.

Evolution of spherical/ellipsoidal vesicles and cylindrical/arachoidal vesicles

To aid in the investigation of the evolution and distinctiveness of spherical/ellipsoidal vesicles and cylindrical/arachoidal vesicles and in the evaluation of the proposed role of these vesicles as cholesterol carriers and donors, we calculated their mean size, surface area, and volume at each of five time points: 6 h and 1, 4, 10, and 20 days (Table 3). The

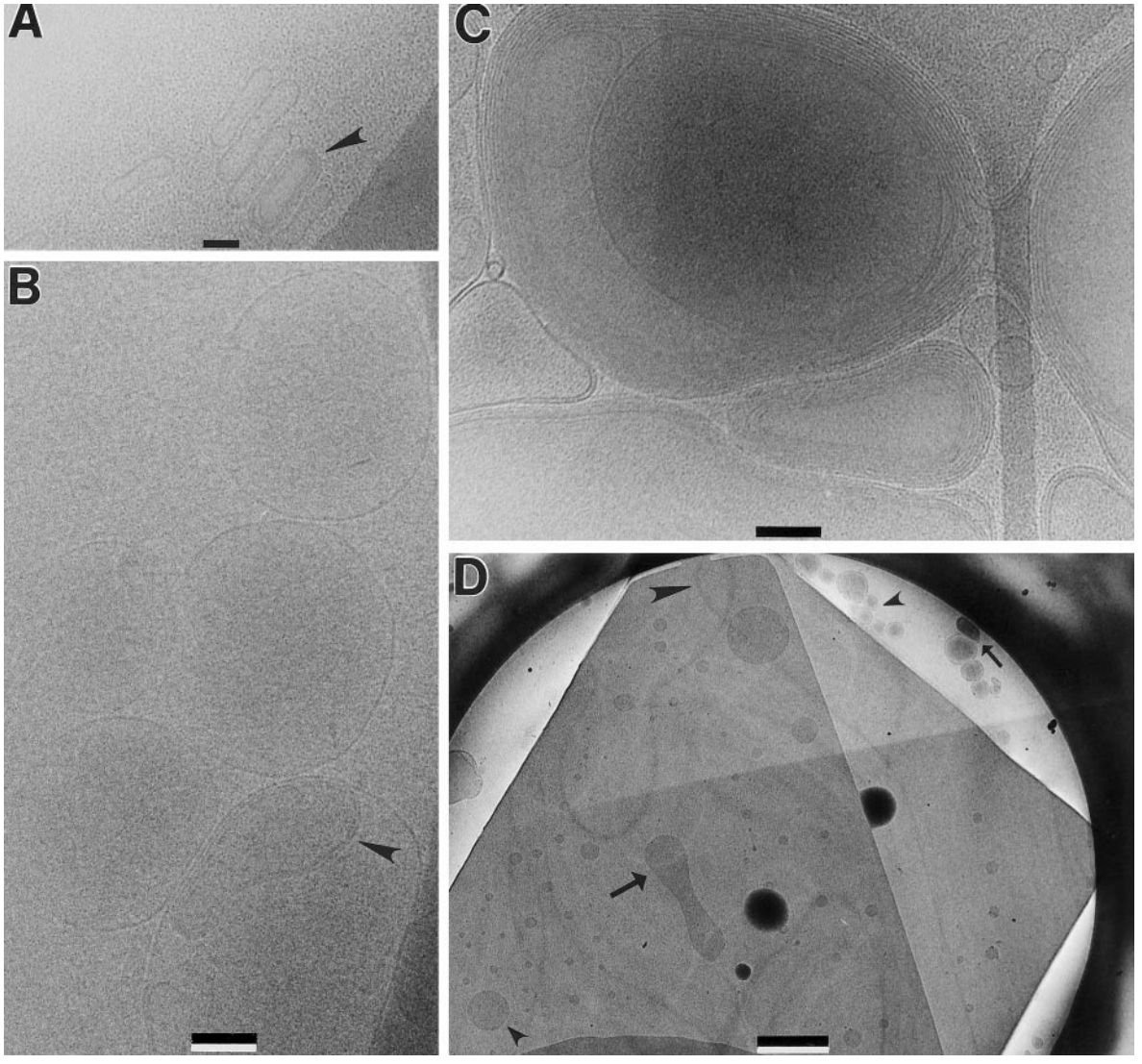

FIGURE 4 Cryo-transmission electron microscopy micrographs of vitreous ice-embedded large unilamellar vesicles, multilamellar vesicles, and cholesterol monohydrate crystals formed in nucleating model bile at various time points after supersaturation by dilution. (*A*) Multilamellar vesicles (*large arrowhead*) observed at 24 h have dimensions of 50 × 140 nm. Cylindrical/arachoidal vesicles and micelles are also visible. Bar = 50 nm. (*B*) Large unilamellar vesicles, shown here at 20 days, had diameters ranging from 140 to 500 nm and may be enlarged because of squeezing/flattening in the vitreous ice layer. Note the multilamellar vesicle inside large unilamellar vesicles (*arrowhead*). The mean bilayer thickness was 5.8 nm. Bar = 100 nm. (*C*) This large multilamellar vesicle seen at 20 days may be of sufficient size (0.64 μm × 0.85 μm) to be identified as a liquid crystal by light microscopy. However, artifactual enlargement is likely because of flattening in thin vitreous ice layers. The mean bilayer thickness was 6.4 nm. Bar = 100 nm. (*D*) A cholesterol monohydrate crystal seen at 20 days had a 8-μm width and characteristic edge angles of 79.2° and 100.8°. Note looped structure (*large arrowhead*), large unilamellar vesicles (*small arrowheads*), multilamellar vesicle (*small arrow*), and a large cylindrical/arachoidal vesicle (*large arrow*). Bar = 1 μm.

mean widths of spherical/ellipsoidal vesicles at 6 h and 4, 10, and 20 days and mean lengths at 6 h and 1, 4, 10, and 20 days (Table 3) were signficantly larger ($p < 0.0005$) than those of primordial vesicles at 23, 27, and 31 min (Table 2). Although some spherical/ellipsoidal vesicles were spherical, the mean shape of spherical/ellipsoidal vesicles was ellipsoidal because mean widths and lengths at all time points were significantly different (Table 3). The mean width, surface area, and volume of spherical/ellipsoidal vesicles increased significantly from 1 to 10 days, then decreased significantly at 20 days. The mean length of spherical/ellipsoidal vesicles increased significantly at 10 days and decreased at 20 days. Within the population of cylindrical/arachoidal vesicles, mean surface area and volume showed a downward trend from 6 h to 10 days.

There was a clear difference between the mean widths and lengths of spherical/ellipsoidal vesicles and cylindrical/arachoidal vesicles (Table 3). In general, the mean surface areas of cylindrical/arachoidal vesicles were larger than those of spherical/ellipsoidal vesicles, and the mean volumes were smaller. The mean surface area and volume of the entire vesicle population were monitored over time by combining and averaging the surface areas and volumes of all spherical/ellipsoidal vesicles and cylindrical/arachoidal

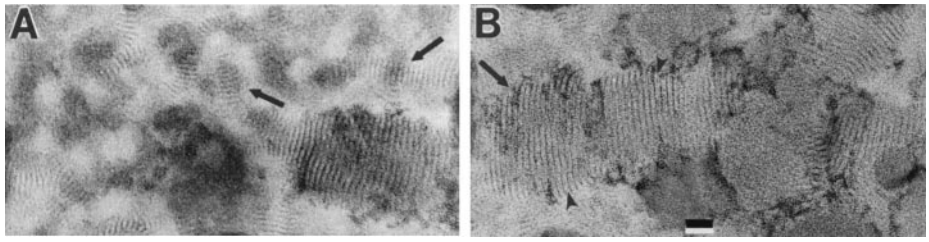

FIGURE 5 Micrographs of fixed (OsO_4) and negatively stained (1% NaPT) model bile sampled from an undisturbed tube at (*a*) 2 days and (*B*) 10 days after supersaturation by dilution. Note lamellar stacks (*arrows*) composed of discs of bilayer thickness 5.0–5.3 nm. Individual layers within the bilayers are visible (*arrowheads*). These lamellar structures were not seen in vitreous ice and are believed to be an artifact. Bar = 25 nm.

vesicles at each time point (Table 4). A significant increase in surface area was noted 10 days after supersaturation, and a significant decrease at 20 days. A surface area/volume ratio (Table 4) of 1:9.0 indicates high volume relative to surface area with a preponderance of spherical/ellipsoidal vesicles, whereas with more cylindrical/arachoidal vesicles present, a ratio of 1:7.3 indicates reduced volume relative to surface area.

The evolution of primordial vesicles, spherical/ellipsoidal vesicles, and cylindrical/arachoidal vesicles can be seen more clearly if the width of each particle is plotted versus the ratio of its width to its length (Fig. 6). Spherical/ellipsoidal vesicles appear at the top of each graph (width/length ratios near 1.0), and elongated cylindrical/arachoidal vesicles near the bottom (ratios $\approx$ 0.2–0.3). Two particles with the same dimensions were superimposed. The distributions of primordial vesicles at 23 and 27 min were similar (Fig. 6, *A* and *B*), as were their mean widths and lengths (Table 2). A portion of the primordial vesicle population at 31 min (Fig. 6 *C*) had diameters 1.5 times the population average. At 6 h (Fig. 6 *D*), the mean diameter of the population of primordial vesicles had increased significantly to a range of 60–90 nm (Table 2). Apparently, that portion of the primordial vesicle population at 31 min that had widths of ~35–55 nm became spherical/ellipsoidal vesicles. No primordial cylindrical/arachoidal vesicles were ever seen. The populations of spherical/ellipsoidal vesicles and cylindrical/arachoidal vesicles each became more homogeneous: the population of spherical/ellipsoidal vesicles evolving toward spheres (Fig. 6, *F* and *H*), and the population of cylindrical/arachoidal vesicles toward longer particles (Fig. 6, *E* and *H*).

The measured populations of spherical/ellipsoidal vesicles and cylindrical/arachoidal vesicles at each time point (Table 3) were combined with additional unmeasured vesicles (unmeasured vesicles were morphologically identified as spherical/ellipsoidal vesicles or cylindrical/arachoidal vesicles, but the images were poorly focused) into a group called "observed" vesicles (Table 5). The frequencies of occurrence of measured and observed spherical/ellipsoidal vesicles and cylindrical/arachoidal vesicles at each time point were in close agreement (Table 5). A χ^2 analysis of the frequency of observed spherical/ellipsoidal vesicles and cylindrical/arachoidal vesicles at the five time points suggested a precursor-product relationship (Table 5): that the changes in ratios of spherical/ellipsoidal vesicles and cylindrical/arachoidal vesicles over time were significant.

DISCUSSION

Cryo-transmission electron microscopy is an excellent technique for observing lipid-rich systems close to their original

TABLE 3 Mean dimensions, surface area, and volume of spherical/ellipsoidal and cylindrical/arachoidal vesicles*

	Spherical/ellipsoidal vesicles					Cylindrical/arachoidal vesicles				
Time	*n*	Width	Length	Surface area	Volume	*n*	Width	Length	Surface area	Volume
6 h	124	54.9 ± 6.7$^{\#}$	62.8 ± 7.4$^{\#\#\P\P}$	10,100 ± 2,300$^{\#}$	102,000 ± 37,000$^{\#}$	62	34.2 ± 5.5***	95.6 ± 24.6§§§	11,900 ± 2,100§****	86,000 ± 20,000***
1 day	69	50.4 ± 7.3§	60.5 ± 6.3§§¶¶	8,700 ± 2,100§	82,000 ± 27,000§	141	29.3 ± 5.2$^{\#\#\#}$	115.3 ± 24.2**	11,800 ± 2,400¶¶¶****	77,000 ± 24,000§§¶¶¶
4 days	122	55.8 ± 8.2¶	62.6 ± 6.4¶¶	10,400 ± 2,700¶	106,000 ± 40,000¶	133	27.3 ± 2.8**	116.9 ± 21.7¶	11,200 ± 2,100	69,000 ± 17,000$^{\#\#\#\#}$
10 days	113	61.5 ± 6.1**	65.8 ± 6.0**¶¶	12,300 ± 2,300**	133,000 ± 36,000**	75	27.8 ± 3.1**	109.3 ± 20.4**	10,700 ± 1,700****	66,000 ± 14,000**$^{\#\#\#\#}$
20 days	114	55.1 ± 4.3	59.6 ± 4.6¶¶	9,900 ± 1,600	96,000 ± 26,000	91	29.9 ± 2.2	101.3 ± 12.0	10,900 ± 1,800****	72,000 ± 18,000$^{\#\#\#\#}$

*Data are expressed as mean ± SD. Units: nm (width and length), nm^2 (surface area), nm^3 (volume). Surface area and volume data have been rounded off. Results of statistical comparisons are based on Ansari-Bradley and Mann-Whitney tests.

$^{\#}p < 0.001$ compared to 1 and 10 days.
$^{\S}p < 0.001$ compared to 4, 10, and 20 days.
$^{\P}p < 0.01$ compared to 10 and 20 days.
$^{**}p < 0.01$ compared to 20 days.
$^{\#\#}p < 0.05$ compared to 1, 10, and 20 days.
$^{\S\S}p < 0.001$ compared to 10 days.
$^{\P\P}p < 0.001$ compared to width of spherical/ellipsoidal vesicles.
$^{***}p < 0.001$ compared to 1, 4, 10, and 20 days.
$^{\#\#\#}p < 0.05$ compared to 4 and 10 days.
$^{\S\S\S}p < 0.001$ compared to 1, 4, and 10 days.
$^{\P\P\P}p < 0.05$ compared to 4 days.
$^{****}p < 0.001$ compared to surface area of spherical/ellipsoidal vesicles.
$^{\#\#\#\#}p < 0.001$ compared to volume of spherical/ellipsoidal vesicles

TABLE 4 Mean surface area and volume of spherical/ellipsoidal and cylindrical/arachoidal vesicles*

Time	*n*	Surface area	Volume	Ratio#
6 h	186	10,700 ± 2,400	96,000 ± 33,000**	1:9.0
1 day	210	10,800 ± 2,700	79,000 ± 25,000##	1:7.3
4 days	255	10,800 ± 2,400	86,000 ± 35,000	1:8.0
10 days	188	11,600 ± 2,200§	106,000 ± 44,000§§	1:9.2
20 days	205	10,300 ± 1,800¶	86,000 ± 26,000	1:8.3

*Measurements of spherical/ellipsoidal and cylindrical/arachoidal vesicles were combined at each time point, then averaged. Data are expressed as mean ± SD. Units: nm^2 (surface area), nm^3 (volume). Surface area and volume data have been rounded off. Results of statistical comparisons are based on Ansari-Bradley and Mann-Whitney tests.
#Surface area:volume.
§$p < 0.001$ compared to 6 h and 1, 4, and 20 days.
¶$p < 0.01$ compared to 6 h and 1 and 4 days.
**$p < 0.01$ compared to 1, 4, 10, and 20 days.
##$p < 0.01$ compared to 4, 10, and 20 days.
§§$p < 0.005$ compared to 4 and 20 days.

state, and our study of a supersaturated nucleating model bile has provided unique observations regarding micelles, intermediate structures, and the evolution of small unilamellar vesicles.

Micelle size and morphology

The size range of micelle width and length was 1.1–5.7 nm and 2.3–10 nm, respectively. These sizes are consistent with coexisting simple and mixed micelles (Cohen and Carey, 1990; Cohen et al., 1993; Mazer et al., 1980). The sizes of simple and mixed micelles in various model systems have been determined by techniques such as quasielastic light scattering (Egelhaaf and Schurtenberger, 1994; Mazer et al., 1979), small-angle neutron scattering (Hjelm et al., 1992; Long et al., 1994b), and small-angle x-ray scattering (Sömjen, 1994) and have previously been summarized (Cohen et al., 1993; Gilat and Sömjen, 1996).

The spherical/globular shape of simple micelles is widely accepted. The shape and structure of mixed micelles are somewhat controversial and are strongly composition dependent (Cabral and Small, 1989). Several models for the structure of bile salt-lecithin mixed micelles have been proposed. The simple disc (Small, 1967) and mixed disc (Mazer et al., 1980) models are one bilayer thick and have axially oriented lecithin with exposed headgroups and a ring of bile salt molecules. Two models of elongated rodlike or "wormlike" micelles have been proposed. The stacked disc model (Shankland, 1970) is composed of repeating units of mixed discs with axially oriented lecithin molecules as mentioned above. A more popular model is an elongated radial shell that has radially oriented lecithin molecules (originally proposed by Ulmius et al., 1982; modified to a capped rod model by Nichols and Ozarowski, 1990; supported by Hjelm et al., 1992). Additional support for the cylindrical or "wormlike" mixed micelle model was provided in egg yolk phosphatidylcholine (EYPC)/octyl glucoside and EYPC/cholate systems by cryo-transmission electron microscopy (Vinson et al., 1989; Walter et al., 1991) and by quasielastic and static light scattering (Cohen et al., 1998). The micelle population in our study appeared generally square to rectangular with occasional rounded ends, suggesting a rodlike or barrel-like morphology. In addition, small, curled, threadlike structures of diameter 1.1–2.2 nm were detected among micelles at 2 min after supersaturation (Fig. 3 *A*).

Intermediate structures

It is well documented that mixed micelles will undergo transition into small unilamellar vesicles upon critical dilution of lecithin-bile salt mixtures (Cabral and Small, 1989; Mazer et al., 1980). The movement of bile salts into the intermicellar space to equalize bile salt concentration after dilution destabilizes the micelles and promotes the formation of intermediate structures such as patches of bilayer (Vinson et al., 1989; Walter et al., 1991), which could lead to the formation of small unilamellar vesicles.

The predominant intermediate structure in our system was denoted as a primordial vesicle. In a model bile of composition similar to ours, low-contrast planar structures were imaged by cryo-TEM at 1 min after dilution (Kaplun et al., 1997). These structures may be analogous to the circular regions of reduced granularity that we observed at 2 min after dilution (Fig. 3 *A*). Although the investigators speculated that these planar structures could be lamellar cholesterol carriers (Sömjen et al., 1990a) or intermediate structures in a micelle-vesicle transition (Walter et al., 1991), no evidence was presented that temporally linked the planar structures to small unilamellar vesicles. We believe that the primordial vesicle is that link.

One of the proposed mechanisms of vesicle assembly and formation is the gradual enlargement of disk-shaped micelles into circular sheetlike, bilayered phospholipid fragments of sufficient size and instability to close upon themselves and form small unilamellar vesicles (Lasic, 1988). This enlargement into larger disks under depleted detergent conditions would require an edge minimization rate as high or higher than the rate of fusion of micelles to the enlarging disk to maintain its smooth, round shape. A two-dimen-

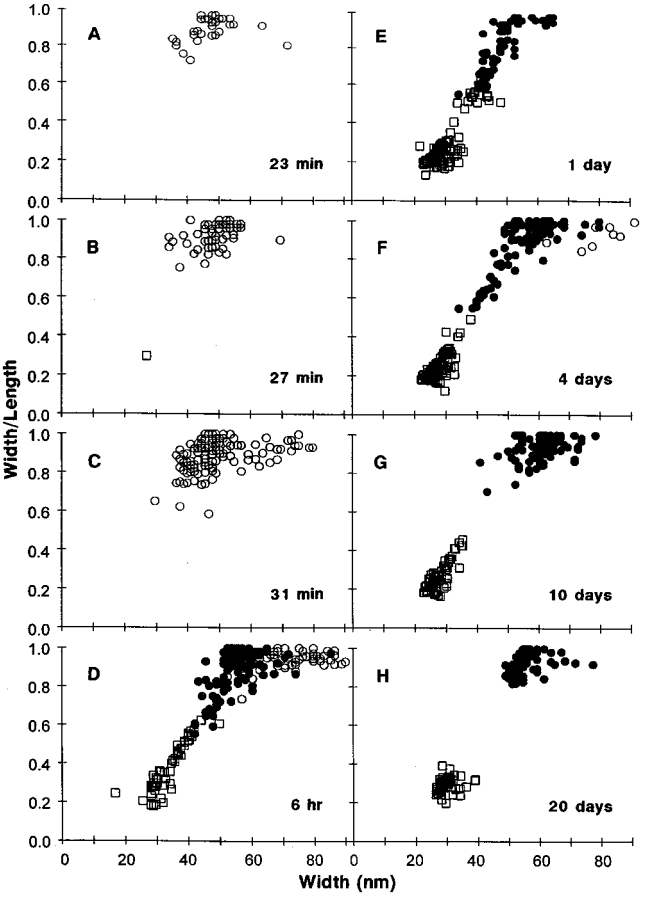

FIGURE 6 Size and morphological evolution of primordial vesicles (○), spherical/ellipsoidal vesicles (●), and cylindrical/arachoidal vesicles (□) with time. (*A*) 23 min, (*B*) 27 min, (*C*) 31 min, (*D*) 6 h, (*E*) 1 day, (*F*) 4 days, (*G*) 10 days, (*H*) 20 days. The actual vesicle width is plotted versus the ratio of width/length. Vesicles with the same dimensions are superimposed. (*A–D, F*) Width/length ratios of primordial vesicles remained constant. The mean size of the population of primordial vesicles increased significantly at 6 h and 4 days compared to 23, 27, and 31 min (Table 2). (*D–H*) The populations of spherical/ellipsoidal vesicles and cylindrical/arachoidal vesicles became more homogeneous with the passage of time (refer to Table 4 for mean sizes).

sional projection of this enlarging disk/sheet would show an intact bilayer around its entire perimeter.

In our model system the presence of cholesterol would increase bilayer viscosity, reduce flexibility of the membrane, and greatly retard spontaneous closure of a round unstable sheet. Therefore, we suggest the following mechanism of vesicle assembly. Upon dilution and loss of bile salts, unstable micelles could fuse at a rate higher than the rate of edge minimization, resulting in a patchwork or framework of small portions of bilayer with many holes between. As this structure grows larger, its inherent flexibility (because it is not a solid sheet) allows a gradual increase in curvature until a three-dimensional structure is formed. A two-dimensional projection of this holey structure would appear as a generally circular primordial vesicle with occasional well-formed bilayer segments such as those seen at 27 min after dilution (Fig. 3 *C*). Some primordial

TABLE 5 Frequencies of observed and measured SEVs and CAVs*

	Observed SUVs#				Measured SUVs§			
	SEVs		CAVs		SEVs		CAVs	
Time	*n*	%	*n*	%	*n*	%	*n*	%
6 hr	509¶	64	288¶	36	124	67	62	33
1 day	388¶	38	626¶	62	69	33	141	67
4 days	632¶	51	611¶	49	122	48	133	52
10 days	487¶	61	306¶	39	113	60	75	40
20 days	424¶	49	436¶	51	114	56	91	44
Total	2440	52	2267	48	542	52	502	48

*SEVs, spherical/ellipsoidal vesicles; CAVs, cylindrical/arachoidal vesicles; SUVs, small unilamellar vesicles.
#Observed SUVs included identifiable SEVs and CAVs in poorly focused micrographs and all measured SUVs. Note similarity of percentages to measured SUVs.
§See Table 3.
¶$p < 0.01$ for χ^2 analysis of frequencies at all five time points; χ^2 value = 153, D.F. = 4.

vesicles viewed at this time point may be sheetlike because they were observed in thin ice toward hole centers (Fig. 3 *C*), and three-dimensional morphology could not be confirmed by 45° tilts. Other primordial vesicles were observed interspersed among small unilamellar vesicles in thicker ice (Fig. 3 *D*). The micelles that appear to be trapped on the inside of young primordial vesicles (Fig. 3 *B*) (these micelles could be outside and be superimposed) as well as micelles on the outside of primordial vesicles would continue to merge with and eventually seal the surface of the forming vesicle. The growth trends of primordial vesicles (Fig. 6, *A–C*) and the diameters of small spherical/ellipsoidal vesicles at 6 h after dilution (Fig. 6 *D*) suggest a gradual enlargement. The larger primordial vesicles seen at 6 h after dilution may produce large unilamellar vesicles, which were seen at later time points (Table 1).

As noted above, primordial vesicles were observed face-on in thin ice most commonly away from hole edges. The extremely rare cluster of lamellae-like structures imaged in Fig. 3 *B* (*arrowhead*) could be an artifact or a group of sheetlike primordial vesicles viewed edge-on in the thicker ice. If these were edge views of primordial vesicles, we would expect to readily detect tangential views, but none were apparent.

Evolution of small unilamellar vesicles

Two distinct morphological populations of small unilamellar vesicles were identified in our system as spherical/ellipsoidal vesicles and cylindrical/arachoidal vesicles. Several investigators have observed small unilamellar vesicles in human biles, as well as in other model biles, suggesting that small unilamellar vesicles have a physiological role, serving as metastable cholesterol carriers (Cohen et al., 1989; Gilat and Sömjen, 1996; Peled et al., 1988). In human hepatic and gallbladder biles from patients with gallstones, spherical/ellipsoidal vesicles were observed using freeze

fracture (Sömjen et al., 1986). The composition of one of the gallbladder biles was 7.5% cholesterol, 18.8% phospholipid, and 73.7% bile salts (all mole %), a composition similar to the model bile used in our study. Kaplun et al. (1994), using cryo-transmission electron microscopy, detected spherical/ellipsoidal vesicles in human gallbladder bile 1 day after collection and visualized spherical/ellipsoidal vesicles and arachoidal vesicles in human hepatic bile, known to contain cholesterol in vesicles (Pattison and Chapman, 1986; Sömjen et al., 1986), at 1, 3, 6, and 9 days after collection. In a model bile of composition 7.5% cholesterol, 12.7% lecithin, and 79.7% sodium cholate (all mol%), Fudim-Levin et al. (1995) observed spherical and arachoidal vesicles by cryo-transmission electron microscopy 6 min after mixing.

Although the initial goals of this study did not involve determining the exact formation time of spherical/ellipsoidal and cylindrical/arachoidal vesicles, the data strongly suggest that spherical/ellipsoidal vesicles preceded cylindrical/arachoidal vesicles for the following reasons: 1) Primordial vesicles of the size and morphology seen 23, 27, and 31 min after dilution (Fig. 3, *B* and *C*; Table 2) would likely become spherical/ellipsoidal vesicles (see 6-h time point in Fig. 3 *D* and Table 3). 2) No primordial vesicles of cylindrical/arachoidal shape were detected. 3) Only one cylindrical/arachoidal vesicle (Fig. 3 *C*, at *arrow*) among 236 spherical/ellipsoidal primordial vesicles was detected at 23, 27, and 31 min (Fig. 3, *B* and *C*, Table 2) within 120 photographed holes.

The mean surface area of the entire population of small unilamellar vesicles was stable for 6 h through 4 days (Table 4), whereas the behavior of the population of spherical/ellipsoidal vesicles was more variable (Table 3). The aggregation/fusion of a portion of the population of spherical/ellipsoidal vesicles with larger size to form multilamellar vesicles could explain the reduction in mean size and surface area of spherical/ellipsoidal vesicles occurring at 1 day (Table 3). However, the subsequent increase in mean size and surface area of the population of spherical/ellipsoidal vesicles noted at 4 days and 10 days (Table 3) when cholesterol monohydrate crystals had commenced to grow, presumably through the fused liquid crystal pathway (Wang and Carey, 1996a), is more difficult to reconcile. We speculate that cholesterol and possibly lecithin was transferred from cylindrical/arachoidal vesicles to spherical/ellipsoidal vesicles (note reduction in surface area of cylindrical/arachoidal vesicles at 4 and 10 days; Table 3). The surface area of the population of spherical/ellipsoidal vesicles decreased significantly at 20 days (Table 3), causing the mean surface area of the entire population of small unilamellar vesicles to reach a minimum (Table 4), whereas the surface area of cylindrical/arachoidal vesicles was not significantly changed (Table 3). This reduction in surface area of spherical/ellipsoidal vesicles likely reflects a major loss of cholesterol utilized in the production of arclike, helical, tubular, and cholesterol monohydrate crystals, which peaked at 18 days (Fig. 2), the latter originating in part from tubular crystals (Wang and Carey, 1996a).

The process of aggregation/fusion of small unilamellar vesicles to form multilamellar vesicles that become visible as liquid crystals by polarizing light microscopy is well supported (Halpern et al., 1986a,b; Kaplun et al., 1997). In our polarizing light microscopy study, small liquid crystals were initially observed at 1 day after supersaturation by dilution (Fig. 2) and disappeared after 14 days. Therefore, we expected to observe by cryo-transmission electron microscopy aggregated and/or partially fused small unilamellar vesicles as well as many multilamellar vesicles. The inability to detect aggregated or partially fused small unilamellar vesicles might be explained in part by agitation before sampling, which could break aggregates, or by their inherent low frequency. In any case, our study provides no insight into how multilamellar structures are formed from unilamellar structures. The multilamellar vesicles that were seen at early time points (1 day in shaken bile, Table 1; 6 h in unshaken bile) were few and of small size (50–150 nm). Multilamellar vesicles as large as those observed by cryo-transmission electron microscopy at 20 days (Fig. 4 *C*) may have been artifactually enlarged by flattening in the ice layer and thus would not have been detectable by polarizing light microscopy (Fig. 2), particularly because small and aggregated liquid crystals lack birefringence (Wang and Carey, 1996a,b). Liquid crystals or liquid crystal aggregates with diameters of several microns would probably not be captured in thin vitreous ice layers because the final sample volume for cryo-transmission electron microscopy was $<0.005\ \mu$l, whereas the sample volume for polarizing light microscopy was $5\ \mu$l.

Not only the existence of multilamellar vesicles in bile in vivo has been confirmed (Wang et al., 1997), but multilamellar vesicles have been observed in human biles that were subsequently incubated in vitro as well as in other model bile systems (Reviewed in Cohen et al., 1993). Multilamellar vesicle-like particles were seen in vitrified samples of human hepatic bile at 9 days after collection (Kaplun et al., 1994). Multilamellar vesicles were visualized by negative stain transmission electron microscopy (a technique prone to artifact with lipid systems) in gallbladder bile that was harvested from the interphase after a $90{,}000 \times g$ centrifugation and incubated in vitro for 2 h (Halpern et al., 1986a). Multilamellar vesicles have also been observed in freeze-fractured preparations of model bile at 5 days of incubation (van de Heijning et al., 1994) and in vitreous ice preparations of 48-h-old model bile (Gilat and Sömjen, 1996).

Potential artifacts

This investigation provides qualitative and quantitative observations of the size and shape of primordial and small unilamellar vesicles in a model bile during a 20-day period after supersaturation. Potential morphological changes, such as invaginations, could occur in vesicles when they are

hyperosmotically stressed in increasing concentrations of NaCl and bile salt during the blotting/previtrification period. Talmon (1996) has provided a useful discussion of some of the artifacts encountered with vitrification of complex fluids.

In our study, sample vitrification was performed in a high-humidity chamber, the use of which has been shown to prevent the formation of invaginations in lipid vesicles (Dubochet et al., 1988) and artifacts in surfactant dispersions (Bellare et al., 1988). Our samples were vitrified on hydrophilic perforated support films, which are known to reduce the evaporation rate (Cyrklaff et al., 1990).

Despite the high-humidity environment surrounding the sample, progressive thinning of the surfactant film will occur after blotting (Frederik et al., 1989). Water loss from the thinner area of the fluid film at the hole center in a perforated carbon film results in a biconcave-shaped film in cross section, which promotes sorting of suspended particles by size and shape (Frederik et al., 1989). Fig. 3 *E* shows an example of this sorting/ranking phenomenon. Biconcave film formation also promotes the concentration of vesicles near the hole edges. Thicker vitreous ice near hole edges did not prevent the acquisition of vesicle images (i.e., Fig. 3, *D* and *E*), enabling us to obtain a representative population of small unilamellar vesicles.

As discussed in Materials and Methods, our pilot study indicated that vitreous ice layers of optimum thickness were obtained with postblotting/preplunging times of 1–10 s. During this period an increased concentration of NaCl could have hyperosmotically stressed vesicles, causing volume reduction and a resultant change in shape (i.e., ellipsoids to cylinders). However, a comparison of the frequencies of each morphological category of small unilamellar vesicles present in each of two aliquots of model bile withdrawn at 1 day after supersaturation but vitrified after two different blotting/preplunging times, 1 and 10 s, indicated that no morphological changes had occurred. The ratios of spherical and ellipsoidal vesicles to cylindrical and arachoidal vesicles were 1:2 at 1 s (48/94) and 10 s (22/46). Investigations by others into osmotic effects on vesicles have focused primarily on the behavior of vesicles in hypotonic solutions (Johnson and Buttress, 1973; Mui et al., 1993).

An increased concentration of taurocholate during the blotting/preplunging period could have promoted dissolution of existing small unilamellar vesicles. Intermediate structures such as bilayer sheets and cylindrical micelles have been observed when phospholipid vesicles were exposed for at least 30 min to concentrations of cholate or octyl glucoside near the micellar phase limit (Cohen et al., 1998; Vinson et al., 1989; Walter et al., 1991). We would not be able to determine whether balanced dissolution of spherical/ellipsoidal vesicles and cylindrical/arachoidal vesicles occurred. However, the fact that the ratio of these vesicle categories was stable at two different postblotting/preplunging times, 1 and 10 s, argues against unequal dissolution.

The relatively recent development of vitreous ice cryomicroscopy (Dubochet et al., 1988) has made it possible to image lipid structures close to their original state in solution. Results obtained with vitreous ice-embedded lipid systems may now be compared to previous studies utilizing negative staining (Howell et al., 1970; Sömjen et al., 1990b), a technique long believed to be prone to artifact in lipid systems (reviewed by Cohen et al., 1993). We believe that the lamellar structures (Fig. 5) produced in negatively stained preparations of our model bile are artifacts, as has been described in a recent review (Carey and Cohen, 1995).

SUMMARY

A supersaturated, nucleating model bile forming three phases (saturated micelles, liquid crystals, and cholesterol monohydrate crystals) was examined by vitreous ice electron microscopy. Micelles, primordial vesicles, two morphologically distinct populations of small unilamellar vesicles categorized as spherical/ellipsoidal vesicles and cylindrical/arachoidal vesicles, multilamellar vesicles, large unilamellar vesicles, and cholesterol monohydrate crystals were observed. Simple and mixed micelles had square/rectangular/ovoid/barrel-like morphology and mean width and length of 3.6 and 5.6 nm. Intermediate structures between micelles and unilamellar spherical/ellipsoidal vesicles were first seen at 23 min after supersaturation and represented the nucleation of primordial vesicles from supersaturated micelles. Subtle changes in primordial vesicle structure such as enlarged micelle-like particles in primordial vesicle interiors, faceted edges, and short segments of bilayer at vesicle peripheries were observed over a time scale of minutes and suggested that vesicle formation in this model bile may be a gradual process involving the merging of micelles to form vesicle boundaries. No evidence of aggregation/fusion of small unilamellar vesicles to form multilamellar vesicles was detected. The accepted role of small unilamellar vesicles as metastable cholesterol carriers and nucleating agents was supported by the inverse correlation of a decrease in mean surface area of small unilamellar vesicles to an increase in production of cholesterol crystals.

We thank Dr. Adrienne Cupples, Professor of Epidemiology and Biostatistics, Boston University School of Public Health, for assistance with statistical analyses. We also thank Ms. Monika M. Leonard for expert technical assistance.

Dr. Wang is a recipient of an Industry Research Scholar Award from the American Digestive Health Foundation/American Gastroenterological Association (1996–1999). This work was supported in part by research and center grants DK 34584 (DQ-HW), DK52911, DK 36588, and DK 34854 (MCC), and HL 26335–17 (DMS), all from the National Institutes of Health (U.S. Public Health Service).

REFERENCES

Bartlett, G. R. 1959. Phosphorous assay in column chromatography. *J. Biol. Chem.* 234:466–468.

Bellare, J. R., H. T. Davis, L. E. Scriven, and Y. Talmon. 1988. Controlled environment vitrification system: an improved sample preparation technique. *J. Electron Microsc. Tech.* 10:87–111.

Cabral, D., and D. M. Small. 1989. Physical chemistry of bile. *In* Handbook of Physiology: The Gastrointestinal System III. S. G. Schultz, J. G. Forte, and B. B. Rauner, editors. American Physiological Society, Waverly Press, Baltimore. 621–662.

Carey, M. C. 1978. Critical tables for calculating the cholesterol saturation of native bile. *J. Lipid Res.* 19:945–955.

Carey, M. C., and D. E. Cohen. 1995. Update on physical state of bile. *Ital. J. Gastroenterol.* 27:92–100.

Carey, M. C., and D. M. Small. 1978. The physical chemistry of cholesterol solubility in bile: relationship to gallstone formation and dissolution in man. *J. Clin. Invest.* 61:998–1026.

Cohen, D. E., M. Angelico, and M. C. Carey. 1989. Quasielastic light scattering evidence for vesicular secretion of biliary lipids. *Am. J. Physiol.* 257:G1–G8.

Cohen, D. E., and M. C. Carey. 1990. Rapid 1 hour high-performance gel filtration chromatography resolves coexisting simple micelles, mixed micelles and vesicles in bile. *J. Lipid Res.* 31:2103–2112.

Cohen, D. E., M. R. Fisch, and M. C. Carey. 1990. Principles of laser light-scattering spectroscopy: applications to the physicochemical study of model and native biles. *Hepatology.* 12:113S–122S.

Cohen, D. E., E. W. Kaler, and M. C. Carey. 1993. Cholesterol carriers in human bile: are "lamellae" involved? *Hepatology.* 18:1522–1532.

Cohen, D. E., G. M. Thurston, R. A. Chamberlin, G. B. Benedek, and M. C. Carey. 1998. Laser light scattering evidence for a common wormlike growth structure of mixed micelles in bile salt- and straight-chain detergent-phosphatidylcholine aqueous systems: relevance to the micellar structure of bile. *Biochemistry.* 37:14798–14814.

Cyrklaff, M., M. Adrian, and J. Dubochet. 1990. Evaporation during preparation of unsupported thin vitrified aqueous layers for cryo-electron microscopy. *J. Electron Microsc. Tech.* 16:351–355.

Dubochet, J., M. Adrian, J. J. Chang, J. C. Homo, J. Lepault, A. W. McDowell, and P. Schultz. 1988. Cryo-electron microscopy of vitrified specimens. *Q. Rev. Biophys.* 21:129–228.

Dubochet, J., M. Groom, and S. Mueller-Neuteboom. 1982. The mounting of macromolecules for electron microscopy with particular reference to surface phenomena and the treatment of support films by glow discharge. *Adv. Opt. Electron Microsc.* 8:107–135.

Egelhaaf, S. V., and P. Schurtenberger. 1994. Shape transformation in the lecithin-bile salt system: from cylinders to vesicles. *J. Phys. Chem.* 98:8560–8573.

Frame, J. S. 1992. Ellipsoid and Spheroid. *In* Encyclopedia of Science and Technology, Vol. 6. McGraw-Hill, New York. 315–316.

Frederik, P. M., M. C. A. Stuart, P. H. H. Bomans, and W. M. Busing. 1989. Phospholipid, nature's own slide and cover slip for cryo-electron microscopy. *J. Microsc.* 153:81–92.

Fromm, H., P. Amin, H. Klein, and I. Kupke. 1980. Use of a simple enzymatic assay for cholesterol analysis in human bile. *J. Lipid Res.* 21:259–261.

Fudim-Levin, E., A. Bor, A. Kaplun, Y. Talmon, and D. Lichtenberg. 1995. Cholesterol precipitation from cholesterol-supersaturated bile models. *Biochim. Biophys. Acta.* 1259:23–28.

Gilat, T., and G. J. Sömjen. 1996. Phospholipid vesicles and other cholesterol carriers in bile. *Biochim. Biophys. Acta.* 1286:95–115.

Groen, A. K., R. Ottenhoff, P. L. M. Jansen, J. van Marle, and G. N. J. Tytgat. 1989. Effect of cholesterol nucleation-promoting activity on cholesterol solubilization in model bile. *J. Lipid Res.* 30:51–58.

Halpern, Z., M. A. Dudley, A. Kibe, M. P. Lynn, A. C. Breuer, and R. T. Holzbach. 1986a. Rapid vesicle formation and aggregation in abnormal human biles. A time-lapse video-enhanced contrast microscopy study. *Gastroenterology.* 90:875–885.

Halpern, Z., M. A. Dudley, M. P. Lynn, J. M. Nader, A. C. Breuer, and R. T. Holzbach. 1986b. Vesicle aggregation in model systems of supersaturated bile: relation to crystal nucleation and lipid composition of the vesicular phase. *J. Lipid Res.* 27:295–306.

Hjelm, R. P., P. Thiyagarajan, and H. Alkan-Onyuksel. 1992. Organization of phosphatidylcholine and bile salt in rodlike mixed micelles. *J. Phys. Chem.* 96:863–866.

Howell, J. I., J. A. Lucy, R. C. Pirola, and I. A. D. Bouchier. 1970. Macromolecular assemblies of lipid in bile. *Biochim. Biophys. Acta.* 210:1–6.

Johnson, S. M., and N. Buttress. 1973. The osmotic insensitivity of sonicated liposomes and the density of phospholipid-cholesterol mixtures. *Biochim. Biophys. Acta.* 307:20–26.

Kaplun, A., F. M. Konikoff, A. Eitan, M. Rubin, A. Vilan, D. Lichtenberg, T. Gilat, and Y. Talmon. 1997. Imaging supramolecular aggregates in bile models and human bile. *Microsc. Res. Tech.* 39:85–96.

Kaplun, A., Y. Talmon, F. M. Konikoff, M. Rubin, A. Eitan, M. Tadmor, and D. Lichtenberg. 1994. Direct visualization of lipid aggregates in native human bile by light- and cryo-transmission electron microscopy. *FEBS Lett.* 340:78–82.

Klösgen, B., and W. Helfrich. 1993. Special features of phosphatidylcholine vesicles as seen in cryo-transmission electron microscopy. *Eur. Biophys. J.* 2:329–340.

Konikoff, F. M., and M. C. Carey. 1994. Cholesterol crystallization from a dilute bile salt-rich model bile. *J. Cryst. Growth.* 144:79–86.

Konikoff, F. M., D. S. Chung, J. M. Donovan, D. M. Small, and M. C. Carey. 1992. Filamentous, helical, and tubular microstructures during cholesterol crystallization from bile. *J. Clin. Invest.* 90:1155–1160.

Lasic, D. D. 1988. The mechanism of vesicle formation. *Biochem. J.* 256:1–11.

Little, T. E., S. P. Lee, H. Madani, E. W. Kaler, and K. Chinn. 1991. Interconversions of lipid aggregates in rat and model bile. *Am. J. Physiol.* 260:G70–G79.

Long, M. A., E. W. Kaler, and S. P. Lee. 1994a. Structural characterization of the micelle-vesicle transition in lecithin-bile salt solutions. *Biophys. J.* 67:1733–1742.

Long, M. A., E. W. Kaler, S. P. Lee, and G. D. Wignall. 1994b. Characterization of lecithin-taurodeoxycholate mixed micelles using small-angle neutron scattering and static and dynamic light scattering. *J. Phys. Chem.* 98:4402–4410.

Mazer, N. A., G. B. Benedek, and M. C. Carey. 1980. Quasielastic light-scattering studies of aqueous biliary lipid systems. Mixed micelle formation in bile salt-lecithin solutions. *Biochemistry.* 19:601–615.

Mazer, N. A., and M. C. Carey. 1983. Quasi-elastic light-scattering studies of aqueous biliary lipid systems. Cholesterol solubilization and precipitation in model bile solutions. *Biochemistry.* 22:426–442.

Mazer, N. A., M. C. Carey, R. F. Kwasnick, and G. B. Benedek. 1979. Quasielastic light scattering studies of aqueous biliary lipid systems. Size, shape, and thermodynamics of bile salt micelles. *Biochemistry.* 18:3064–3075.

Mui, B. L.-S., P. R. Cullis, E. A. Evans, and T. D. Madden. 1993. Osmotic properties of large unilamellar vesicles prepared by extrusion. *Biophys. J.* 64:443–453.

Mui, B. L.-S., H.-G. Dobereiner, T. D. Madden, and P. R. Cullis. 1995. Influence of transbilayer area asymmetry on the morphology of large unilamellar vesicles. *Biophys. J.* 69:930–941.

Nichols, J. W., and J. Ozarowski. 1990. Sizing of lecithin-bile salt mixed micelles by size-exclusion high-performance liquid chromatography. *Biochemistry.* 29:4600–4606.

Pattison, N., and B. Chapman. 1986. Distribution of biliary cholesterol between mixed micelles and non-micelles in relation to fasting and feeding in humans. *Gastroenterology.* 91:697–702.

Peled, Y., Z. Halpern, R. Baruch, G. Goldman, and T. Gilat. 1988. Cholesterol nucleation from its carriers in human bile. *Hepatology.* 8:914–918.

Pope, J. L. 1967. Crystallization of sodium taurocholate. *J. Lipid Res.* 8:146–147.

Shankland, W. 1970. The equilibrium and structure of lecithin-cholate mixed micelles. *Chem. Phys. Lipids.* 4:109–130.

Small, D. M. 1967. Physico-chemical studies of cholesterol gallstone formation. *Gastroenterology.* 52:607–610.

Small, D. M. 1980. Cholesterol nucleation and growth in gallstone formation. *N. Engl. J. Med.* 302:1305–1307.

Small, D. M. 1986. Sterols and Sterol Esters. *In* The Physical Chemistry of Lipids from Alkanes to Phospholipids. Plenum Press, New York. 395–406.

Sömjen, G. 1994. New concepts in bile salt/phospholipid systems. *In* Theory and Applications. Swiss Society for Biochemistry, Swiss Biophysical Society, Swiss Group of Colloid and Interface Science and Hoffmann-LaRoche International Symposium, Basel, May.

Sömjen, G. J., Y. Marikovsky, P. Lelkes, and T. Gilat. 1986. Cholesterol-phospholipid vesicles in human bile: an ultrastructural study. *Biochim. Biophys. Acta.* 879:14–21.

Sömjen, G. J., Y. Marikovsky, E. Wachtel, P. R. C. Harvey, R. Rosenberg, S. M. Strasberg, and T. Gilat. 1990a. Phospholipid lamellae are cholesterol carriers in human bile. *Biochim. Biophys. Acta.* 1042:28–35.

Sömjen, G. J., R. Rosenberg, and T. Gilat. 1990b. Gel filtration and quasielastic light scattering studies of human bile. *Hepatology.* 12: 123S–129S.

Talmon, Y. 1996. Transmission electron microscopy of complex fluids: the state of the art. *Ber. Bunsenges. Phys. Chem.* 100:364–372.

Tao, S., S. Tazuma, and G. Kajiyana. 1993. Apolipoprotein A-I stabilizes phospholipid lamellae and thus prolongs nucleation time in model bile systems: an ultrastructural study. *Biochim. Biophys. Acta.* 1166:25–30.

Toor, E. W., D. F. Evans, and E. L. Cussler. 1978. Cholesterol monohydrate growth in model bile solutions. *Proc. Natl. Acad. Sci. USA.* 75:6230–6234.

Toyoshima, C. 1989. On the use of holey grids in electron crystallography. *Ultramicroscopy.* 30:439–444.

Turley, S. D., and J. M. Dietschy. 1978. Re-evaluation of the 3α-hydroxysteroid dehydrogenase assay for total bile acids in bile. *J. Lipid Res.* 19:924–928.

Ulmius, J., G. Lindblom, H. Wennerström, L. B.-A. Johansson, K. Fontell, O. Söderman, and G. Arvidson. 1982. Molecular organization in the liquid-crystalline phases of lecithin-sodium cholate-water systems studied by nuclear magnetic resonance. *Biochemistry.* 21:1553–1560.

van de Heijning, B. J. M., M. F. J. Stolk, K. J. van Erpecum, W. Renooij, and G. P. van Berge Henegouwen. 1994. The effects of bile salt hydrophobicity on model bile vesicle morphology. *Biochim. Biophys. Acta.* 1212:203–210.

Vinson, P. K., Y. Talmon, and A. Walter. 1989. Vesicle-micelle transition of phosphatidylcholine and octyl glucoside elucidated by cryo-transmission electron microscopy. *Biophys. J.* 56:669–681.

Walter, A., P. K. Vinson, A. Kaplun, and Y. Talmon. 1991. Intermediate structures in the cholate-phosphatidylcholine vesicle-micelle transition. *Biophys. J.* 60:1315–1325.

Wang, D. Q-H., and M. C. Carey. 1996a. Complete mapping of crystallization pathways during cholesterol precipitation from model bile: influence of physical-chemical variables of pathophysiologic relevance and identification of a stable liquid crystalline state in cold, dilute and hydrophilic bile salt-containing systems. *J. Lipid Res.* 37:606–630.

Wang, D. Q-H., and M. C. Carey. 1996b. Characterization of crystallization pathways during cholesterol precipitation from human gallbladder biles: identical pathways to corresponding model biles with three predominating sequences. *J. Lipid Res.* 37:2539–2549.

Wang, D. Q-H., B. Paigen, and M. C. Carey. 1997. Phenotypic characterization of *Lith* genes that determine susceptibility to cholesterol cholelithiasis in inbred mice: physical chemistry of gallbladder bile. *J. Lipid Res.* 38:1395–1411.